Measurement of Ribose Carbon Chemical Shift Tensors for A-form RNA by Liquid Crystal NMR Spectroscopy

David L. Bryce,[†] Alexander Grishaev, and Ad Bax*

Contribution from the Laboratory of Chemical Physics, National Institute of Diabetes and Digestive and Kidney Diseases, National Institutes of Health, Bethesda, Maryland 20892

Received February 17, 2005; E-mail: bax@nih.gov

Abstract: Incomplete motional averaging of chemical shift anisotropy upon weak alignment of nucleic acids and proteins in a magnetic field results in small changes in chemical shift. Knowledge of nucleus-specific chemical shift (CS) tensor magnitudes and orientations is necessary to take full advantage of these measurements in biomolecular structure determination. We report the determination by liquid crystal NMR of the CS tensors for all ribose carbons in A-form helical RNA, using a series of novel 3D NMR pulse sequences for accurate and resolved measurement of the ribose ^{13}C chemical shifts. The orientation of the riboses relative to the rhombic alignment tensor of the molecule studied, a stem-loop sequence corresponding to helix-35 of 23S rRNA, is known from an extensive set of residual dipolar couplings (RDC), previously used to refine its structure. Singular-value-decomposition fits of the chemical shift changes to this structure, or alternatively to a database of helical RNA X-ray structures, provide the CS tensor for each type of carbon. Quantum chemical calculations complement the experimental results and confirm that the most shielded tensor component lies approximately along the local carbon–oxygen bond axis in all cases and that shielding anisotropy for C3′ and C4′ is much larger than for C1′ and C2′, with C5′ being intermediate.

Introduction

The study of the structure and dynamics of biological molecules such as proteins and nucleic acids by NMR spectroscopy has conventionally relied upon semiquantitative local restraints such as NOEs and *J* couplings.[1] However, traditional NMR structures of nucleic acids in particular suffer due to their extended form and the resultant paucity of useful long-range NOE data.[2–4] Weak alignment of DNA and RNA in the magnetic field, in combination with isotopic enrichment procedures, has allowed for new types of NMR measurements which offer a more precise definition of nucleic acid structure in solution, in particular regarding the global properties such as bending and relative orientation of helices.[5–10] Such measurements are made by dissolving the nucleic acid in a liquid crystalline aligning medium,[11–13] by aligning it in an anisotro-

pically compressed hydrogel,[14–16] or by taking advantage of the intrinsic magnetic susceptibility anisotropy of the molecules themselves.[17–22] Under these conditions, orientation-dependent second-rank tensors, such as the dipolar coupling and the chemical shift (CS) tensor, no longer average to their isotropic values. A residual dipolar coupling (RDC) between a pair of nuclear spins then provides precise information on the orientation of the corresponding internuclear vector relative to the molecular alignment tensor. One-bond $^{13}C-^1H$, $^{15}N-^1H$, $^{13}C-^{13}C$, and $^{13}C-^{15}N$ RDCs are particularly useful in this regard. The weak alignment technology, along with additional important recent advances,[23–27] has facilitated the study of

† Current address: Department of Chemistry, University of Ottawa, Ottawa, Ontario K1N 6N5, Canada.

(1) Wüthrich, K. *NMR of Proteins and Nucleic Acids*; John Wiley & Sons: New York, 1986.
(2) Metzler, W.; Wang, C.; Kitchen, D.; Levy, R.; Pardi, A. *J. Mol. Biol.* **1990**, *214*, 711–736.
(3) Ulyanov, N. B.; Gorin, A. A.; Zhurkin, V. B.; Chen, B. C.; Sarma, M. H.; Sarma, R. H. *Biochemistry* **1992**, *31*, 3918–3930.
(4) Allain, F. H. T.; Varani, G. *J Mol. Biol.* **1997**, *267*, 338–351.
(5) Mollova, E. T.; Hansen, M. R.; Pardi, A. *J. Am. Chem. Soc.* **2000**, *122*, 11561–11562.
(6) Bayer, P.; Varani, L.; Varani, G. *J. Biomol. NMR* **1999**, *14*, 149–155.
(7) Sibille, N.; Pardi, A.; Simorre, J. P.; Blackledge, M. *J. Am. Chem. Soc.* **2001**, *123*, 12135–12146.
(8) Stefl, R.; Wu, H. H.; Ravindranathan, S.; Sklenar, V.; Feigon, J. *Proc. Natl. Acad. Sci. U.S.A.* **2004**, *101*, 1177–1182.
(9) MacDonald, D.; Lu, P. *Curr. Opin. Struct. Biol.* **2002**, *12*, 337–343.
(10) Barbic, A.; Zimmer, D. P.; Crothers, D. M. *Proc. Natl. Acad. Sci. U.S.A.* **2003**, *100*, 2369–2373.
(11) Tjandra, N.; Bax, A. *Science* **1997**, *278*, 1111–1114.
(12) Hansen, M. R.; Mueller, L.; Pardi, A. *Nat. Struct. Biol.* **1998**, *5*, 1065–1074.
(13) Clore, G. M.; Starich, M. R.; Gronenborn, A. M. *J. Am. Chem. Soc.* **1998**, *120*, 10571–10572.
(14) Sass, H. J.; Musco, G.; Stahl, S. J.; Wingfield, P. T.; Grzesiek, S. *J. Biomol. NMR* **2000**, *18*, 303–309.
(15) Tycko, R.; Blanco, F. J.; Ishii, Y. *J. Am. Chem. Soc.* **2000**, *122*, 9340–9341.
(16) Kim, I.; Lukavsky, P. J.; Puglisi, J. D. *J. Am. Chem. Soc.* **2002**, *124*, 9338–9339.
(17) Kung, H. C.; Wang, K. Y.; Goljer, I.; Bolton, P. H. *J. Magn. Reson Ser. B* **1995**, *109*, 323–325.
(18) Gayathri, C.; Bothnerby, A. A.; Vanzijl, P. C. M.; Maclean, C. *Chem. Phys. Lett.* **1982**, *87*, 192–196.
(19) Bryce, D. L.; Boisbouvier, J.; Bax, A. *J. Am. Chem. Soc.* **2004**, *126*, 10820–10821.
(20) Al-Hashimi, H. M.; Tolman, J. R.; Majumdar, A.; Gorin, A.; Patel, D. J. *J. Am. Chem. Soc.* **2001**, *123*, 5806–5807.
(21) Van Buuren, B. N. M.; Schleucher, A.; Wittmann, V.; Griesinger, C.; Schwalbe, H.; Wijmenga, S. S. *Angew. Chem., Int. Ed.* **2004**, *43*, 187–192.
(22) Zhang, Q.; Throolin, R.; Pitt, S. W.; Serganov, A.; Al-Hashimi, H. M. *J. Am. Chem. Soc.* **2003**, *125*, 10530–10531.
(23) Clore, G. M.; Kuszewski, J. *J. Am. Chem. Soc.* **2003**, *125*, 1518–1525.
(24) Reif, B.; Hennig, M.; Griesinger, C. *Science* **1997**, *276*, 1230–1233.

structure and dynamics of RNAs as large as 30 kDa.[28−31] Recently, the practicality and utility of experiments which allow for the measurement of $^1H-^1H$ RDCs over a distance of up to 12 Å have also been reported for a DNA dodecamer.[32]

With the increasing availability of high-field commercial NMR spectrometers (e.g., 800, 900 MHz and beyond), the impact of the anisotropic CS tensor (δ) on NMR spectra and relaxation is becoming more prominent due to its scaling (in hertz) with the magnetic field strength, B_0. The difference in apparent chemical shifts observed for weakly aligned (δ_{aniso}) and isotropic (δ_{iso}) samples, is given by:

$$\Delta\delta = \delta_{aniso} - \delta_{iso} = \sum_{i=x,y,z} \sum_{j=x,y,z} A_{jj} \cos^2(\theta_{ij})\delta_{ii} \quad (1)$$

where A_{jj} are the principal components of the molecular alignment tensor, δ_{ii} are the principal components of the CS tensor, and θ_{ij} is the angle between the jj axis of the alignment tensor and the ii axis of the CS tensor. For the magnitude of alignment typically used in biomolecular NMR, $10^{-4}-10^{-3}$, the measured $\Delta\delta$ are on the order of parts per billion (ppb).

Chemical shift changes, $\Delta\delta$, resulting from incomplete averaging of the effect of chemical shift anisotropy, below simply referred to as anisotropic shifts, have previously been measured for carbonyl $^{13}C'$ and amide ^{15}N nuclei in the protein ubiquitin and were used to determine the magnitude and orientation of their average CS tensors by means of a systematic grid search.[33] Equally as important, it has been demonstrated that measurements of $\Delta\delta$ are very useful in the validation and refinement of protein structures.[34−36] More recently, site-specific carbonyl ^{13}C CS tensors have been characterized for ubiquitin by Markwick and Sattler[37] and by Bodenhausen and co-workers.[38] To date, only ^{31}P anisotropic shifts have been used successfully for nucleic acid structure refinement and valida-tion.[39−41] The principal components and orientations used in these studies were estimated from solid-state NMR studies on model systems such as barium diethyl phosphate.[42]

Given the large number of torsion-angle variables required to define the geometry of a given nucleotide in RNA, additional experimental anisotropic CS restraints would be desirable to increase the precision and accuracy of RNA structures deter-mined by solution NMR. Furthermore, knowledge of the CS tensors will be valuable for the interpretation of cross-correlated relaxation effects. The magnitude but not the orientations of the ribose and deoxyribose ^{13}C chemical shift tensors of several mononucleotides have recently been determined by FIREMAT solid-state NMR experiments.[43]

Here, we report the average magnitudes and orientations of the chemical shift tensors for the five ribose carbons (C1′, C2′, C3′, C4′, and C5′) of A-form helical RNA, determined by using liquid crystal NMR spectroscopy. The experimental results are complemented with a series of quantum chemical calculations of the CS tensors.

Experimental Section

Sample Preparation. Two samples of a uniformly $^{13}C,^{15}N$-enriched 24-nucleotide stem-loop RNA oligomer derived from helix-35 of *Escherichia coli* 23S ribosomal RNA and modified with pseudouridine (ψ) at the position corresponding to residue 746 were used (Figure 1A). The nucleotide sequence, r(GGGCUAAUGψUGAAAAA-UUAGCCC), is labeled as G37−C60 in this contribution (instead of G737−C760). Sample preparation has been described previously.[44] Briefly, the samples were prepared in identical fashion in Shigemi microcells (300 μL), and each contained 1.5 mM helix-35ψ, 17 mM NaCl, 17 mM potassium phosphate, and 0.03 mM EDTA in 99% D$_2$O at pH 6.8. One of the samples contained 25 mg/mL filamentous phage Pf1,[12] purchased from Asla Biotech Ltd. (Riga, Latvia, http://www.asla-biotech.com). The ^2H lock solvent quadrupole splitting observed for the Pf1-aligned sample was 28.3 Hz at 298 K. To obtain reliable anisotropic chemical shift measurements, particular care was taken to ensure that both samples are prepared with identical salt concentrations and pH, thereby minimizing the effects of differential sample conditions on the chemical shifts.

NMR Spectroscopy. NMR spectra were recorded at 298 K on a Bruker DRX800 spectrometer equipped with a triple-resonance cryo-genic probehead with z-axis pulsed field gradients, and on a Bruker DMX750 spectrometer equipped with a triple-resonance room-tem-perature, three-axis pulsed field gradient probehead. One-bond C1′−H1′ and C2′−H2′ RDCs were measured using the H1C1C2 experiment.[45] Fitting of these RDCs by means of singular value decomposition (SVD) to an NMR-refined structure of helix-35ψ was used to determine the magnitude and orientation of the alignment tensor of the molecule.[46,47] Except for a scaling factor of 1.4, which accounts for the higher Pf1 concentration used in the present study, the alignment tensor was found to be identical to that obtained from a previous sample preparation.[45]

Isotropic and anisotropic C1′ chemical shifts were measured using a 2D double-constant-time (50 ms, corresponding to 555 complex points in t_1) HSQC pulse sequence. The gradient-and-sensitivity-enhanced version[48] and a WATERGATE[49] version of the sequence were employed. No systematic differences in the observed liquid-crystal-induced shifts, $\Delta\delta = \delta_{aniso} - \delta_{iso}$, were observed to result from the reconversion scheme used in the HSQC experiment, nor from the type of probehead.

(25) Tu, K. C.; Gochin, M.; Kollman, P. *FASEB J.* **1997**, *11*, A835−A835.
(26) Boisbouvier, J.; Gans, P.; Blackledge, M.; Brutscher, B.; Marion, D. *J. Am. Chem. Soc.* **1999**, *121*, 7700−7701.
(27) Chiarparin, E.; Rudisser, S.; Bodenhausen, G., *ChemPhysChem* **2001**, *2*, 41−45.
(28) Lukavsky, P. J.; Kim, I.; Otto, G. A.; Puglisi, J. D. *Nat. Struct. Biol.* **2003**, *10*, 1033−1038.
(29) Leeper, T.; Leulliot, N.; Varani, G. *Nucleic Acids Res.* **2003**, *31*, 2614−2621.
(30) Lawrence, D. C.; Stover, C. C.; Noznitsky, J.; Wu, Z. R.; Summers, M. F. *J. Mol. Biol.* **2003**, *326*, 529−542.
(31) Wu, H. H.; Henras, A.; Chanfreau, G.; Feigon, J. *Proc. Natl. Acad. U.S.A.* **2004**, *101*, 8307−8312.
(32) Boisbouvier, J.; Delaglio, F.; Bax, A. *Proc. Natl. Acad. U.S.A.* **2003**, *100*, 11333−11338.
(33) Cornilescu, G.; Bax, A. *J. Am. Chem. Soc.* **2000**, *122*, 10143−10154.
(34) Lipsitz, R. S.; Tjandra, N. *J. Magn. Reson* **2003**, *164*, 171−176.
(35) Cornilescu, G.; Marquardt, J. L.; Ottiger, M.; Bax, A. *J. Am. Chem. Soc.* **1998**, *120*, 6836−6837.
(36) Tugarinov, V.; Kay, L. E. *J. Mol. Biol.* **2003**, *327*, 1121−1133.
(37) Markwick, P. R. L.; Sattler, M. *J. Am. Chem. Soc.* **2004**, *126*, 11424−11425.
(38) Cisnetti, F.; Loth, K.; Pelupessy, P.; Bodenhausen, G. *ChemPhysChem* **2004**, *5*, 807−814.
(39) Wu, Z. R.; Tjandra, N.; Bax, A. *J. Am. Chem. Soc.* **2001**, *123*, 3617−3618.
(40) O'Neil-Cabello, E.; Wu, Z.; Bryce, D. L.; Nikonowicz, E. P.; Bax, A. *J. Biomol. NMR* **2004**, *30*, 61−70.
(41) Wu, Z.; Delaglio, F.; Tjandra, N.; Zhurkin, V. B.; Bax, A. *J. Biomol. NMR* **2003**, *26*, 297−315.
(42) Herzfeld, J.; Griffin, R. G.; Haberkorn, R. A. *Biochemistry* **1978**, *17*, 2711−2718.

(43) Stueber, D.; Grant, D. M.,*J. Am. Chem. Soc.* **2002**, *124*, 10539−10551.
(44) Jaroniec, C. P.; Boisbouvier, J.; Tworowska, I.; Nikonowicz, E. P.; Bax, A. *J. Biomol. NMR* **2005**, *31*, 231−241.
(45) O'Neil-Cabello, E.; Bryce, D. L.; Nikonowicz, E. P.; Bax, A. *J. Am. Chem. Soc.* **2004**, *126*, 66−67.
(46) Losonczi, J. A.; Andrec, M.; Fischer, M. W. F.; Prestegard, J. H. *J. Magn. Reson* **1999**, *138*, 334−342.
(47) Sass, J.; Cordier, F.; Hoffmann, A.; Rogowski, M.; Cousin, A.; Omichinski, J. G.; Lowen, H.; Grzesiek, S. *J. Am. Chem. Soc.* **1999**, *121*, 2047−2055.
(48) Kay, L. E.; Keifer, P.; Saarinen, T. *J. Am. Chem. Soc.* **1992**, *114*, 10663−10665.
(49) Piotto, M.; Saudek, V.; Sklenár, V. *J. Biomol. NMR* **1992**, *2*, 661−665.
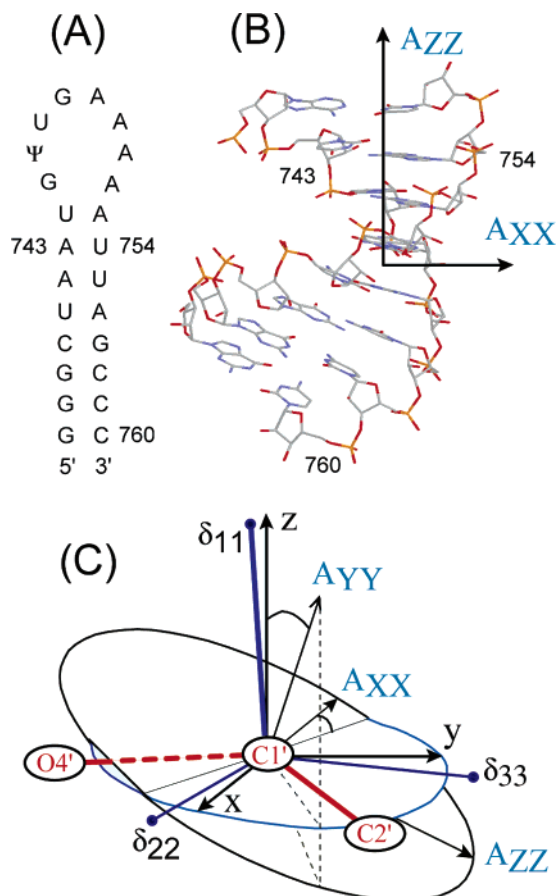
Figure 1. (A) Sequence of the 24-nt helix-35ψ RNA studied. (B) Typical NMR-refined structure of the A-form helical stem portion of helix-35ψ RNA (G37-U44; A53-C60), with the molecular alignment tensor axes superimposed. The view is along the A_{YY} axis. Hydrogen atoms have been omitted for clarity. (C) Example (for C1′ in a given nucleotide) of the relationship between the three axis systems used in this paper. The molecular alignment tensor axes for the molecule are labeled as in part (B), A_{XX}, A_{YY}, and A_{ZZ}. An arbitrary local axis system (x,y,z) is defined for C1′ such that the x-axis bisects the O4′−C1′−C2′ angle, the y-axis lies in the same plane, and the z-axis is perpendicular to this plane. In the case of C1′, the most shielded component of the CS tensor, δ_{33}, lies approximately along the y-axis of the reference system, δ_{22} approximately along x, and δ_{11} approximately along z. In the more general case, the diagram appears more complicated since the CS tensor PAS does not necessarily coincide so closely with the arbitrary xyz axis system. For each nucleotide, the xyz axis system and the CS tensor PAS are constant, while the orientation of A will be different.

Isotropic and anisotropic chemical shifts for C2′, C3′, and C4′ were measured using a series of related out-and-back 3D NMR experiments: proton-decoupled H1C1C2, H1C1(C2)C3, and H1C1-(C2C3)C4 (Figure 2A). Data matrices for these three experiments consisted of 29 (t_1) × 39 (t_2) × 512 (t_3) complex data points. The proton carrier was placed on the residual HDO resonance, and the ^{13}C carrier was typically placed at 82 ppm. The change in lock field frequency in the aligned sample due to locking on one of the two ^{2}H doublet components was accounted for by adjusting the ^{1}H and ^{13}C carrier frequencies appropriately for the aligned sample, e.g., a change in ^{1}H frequency of −91.70 Hz necessitated a change of −91.70(γ_{13C}/γ_{1H}) = −23.06 Hz for ^{13}C.

Isotropic and anisotropic chemical shifts for C5′ were measured using a "straight-through" (H5)C5(C4C3C2)C1H1 pulse sequence (Figure 2B). Datasets consisted of 28 (t_1) × 39 (t_2) × 512 (t_3) complex data points.

All spectra were processed and analyzed using nmrPipe.[50] No linear prediction was used in the processing schemes to ensure the most accurate chemical shifts were obtained. The indirect dimension time-

domain data were apodized using a squared cosine bell function truncated at 77.4°. Time-domain data in the ^{1}H dimension were zero-filled to 2k; time-domain data in the indirect dimensions of the 3D experiments were zero-filled to 128 or 256 points. Time-domain data in the ^{13}C dimension of the 2D HSQC experiments were zero-filled to 2k. Particular care was taken in the phasing of the spectra,[52] and manual phasing of each peak was found to be necessary in the case of the C5′ measurements as minute (<5°) phase distortions were found to have a noticeable effect on peak positions.

At least two replicate measurements of all datasets were made over a period of six weeks to estimate the precision of the results and improve them by averaging. The ^{2}H lock splitting was checked frequently, and remained constant within 0.1 Hz over this period.

Quantum Chemical Calculations. All calculations were carried out using Gaussian03[53] running on the Helix and Biowulf PC/Linux clusters at the National Institutes of Health. Calculations were performed on individual guanidine and cytidine nucleotide fragments, consisting of base, sugar, and phosphate moieties. The initial geometries were taken from the high-resolution X-ray structure of an A-form RNA helix (PDB 1QCU[54]) and have a pseudorotation phase, P, amplitude, ψ_m, and glycosidic torsion angle χ of (13°, 45°, −159°) and (15°, 47°, −161°), respectively for G and C. Additional calculations (Supporting Information) were carried out for a C1′-exo guanidine (130°, 41°, −82°). Experimental torsion angle restraints defining the backbone, sugar, and glycosidic bond were enforced during a partial geometry optimization at the B3LYP/6-311G* level in order to maintain the A-form geometry (Supporting Information). The optimization resulted in minor changes in bond lengths and angles, and provided proper proton positions with respect to the heavy atoms. Nuclear magnetic shielding tensor calculations were carried out on the optimized structures using restricted Hartree−Fock (RHF) theory, density functional theory (DFT) using the PBE exchange and correlation functionals,[55,56] or alternatively using the B3LYP hybrid functional.[57] The following basis sets were used on all atoms in separate calculations: 6-311+G*, 6-311++G**, and cc-pVTZ. The gauge-including atomic orbitals (GIAO) method[58,59] was used in all cases. The resulting symmetric parts of the magnetic shielding tensors were diagonalized to determine their principal components and orientations with respect to the molecular framework.

Results and Discussion

Measurement of Ribose Carbon Anisotropic Chemical Shifts. Experimental values of $\Delta\delta(^{13}C)$ for the ribose carbons determined from NMR measurements on isotropic and aligned samples of helix-35ψ RNA are presented in Table 1. These measurements were carried out using the pulse sequences shown in Figure 2, as well as a double-constant-time HSQC experiment for the well-resolved C1′ resonances. The sequences shown in Figure 2A are proton-decoupled extensions of the previously published H1C1C2 experiment,[45] in which magnetization originating on H1′ is transferred via multiple-quantum coherence through C1′ to C2′. Depending on the number of 12.5-ms ^{13}C−^{13}C relay steps used, magnetization then evolves during a

(50) Delaglio, F.; Grzesiek, S.; Vuister, G. W.; Zhu, G.; Pfeifer, J.; Bax, A. *J. Biomol. NMR* **1995**, *6*, 277−293.
(51) Geen, H.; Freeman, R. *J. Magn. Reson* **1991**, *93*, 93−141.
(52) Kontaxis, G.; Clore, G. M.; Bax, A. *J. Magn. Reson.* **2000**, *143*, 184−196.
(53) Frisch, M. J. et al. *Gaussian03*, Revision C02; Gaussian Inc.: Wallingford CT, 2004.
(54) Klosterman, P. S.; Shah, S. A.; Steitz, T. A. *Biochemistry* **1999**, *38*, 14784−14792.
(55) Perdew, J. P.; Burke, K.; Ernzerhof, M. *Phys. Rev. Lett.* **1996**, *77*, 3865−3868.
(56) Perdew, J. P.; Burke, K.; Ernzerhof, M. *Phys. Rev. Lett.* **1997**, *78*, 1396−1396.
(57) Becke, A. D. *J. Chem. Phys.* **1993**, *98*, 5648−5652.
(58) Ditchfield, R. *Mol. Phys.* **1974**, *27*, 789−807.
(59) Wolinski, K.; Hinton, J. F.; Pulay, P. *J. Am. Chem. Soc.* **1990**, *112*, 8251−8260.
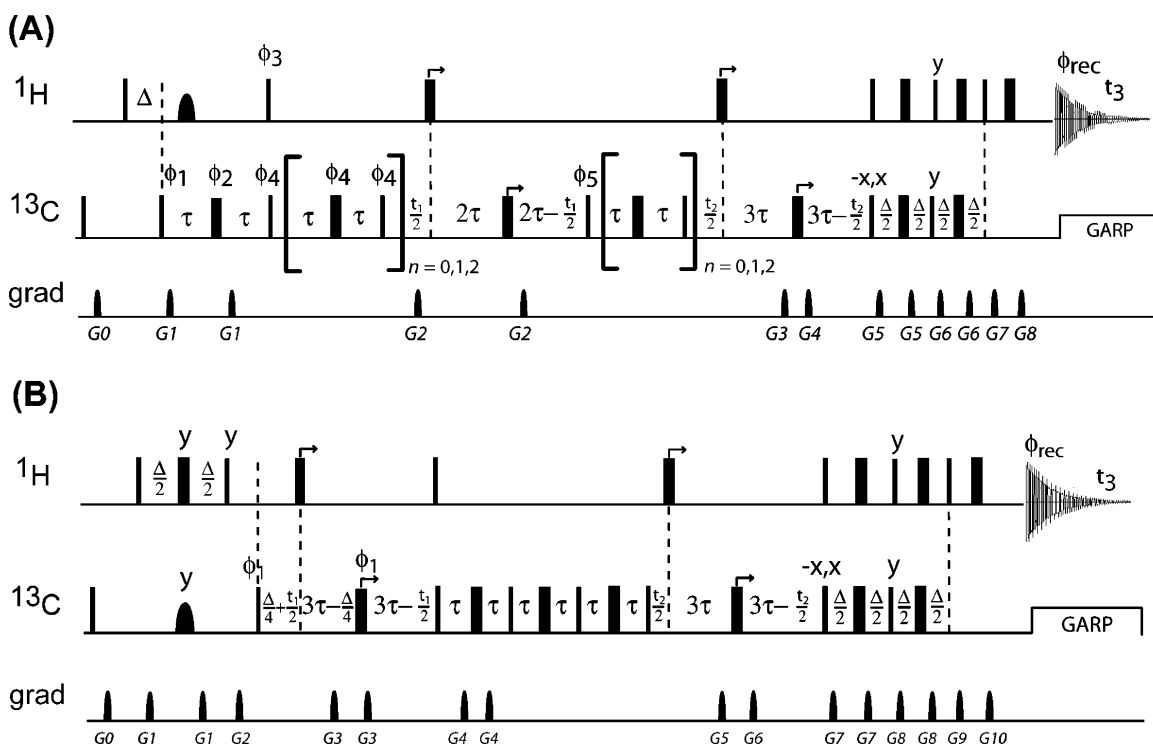
Figure 2. (A) Proton-decoupled out-and-back H1C1C2 ($n = 0$), H1C1(C2)C3 ($n = 1$), and H1C1(C2C3)C4 ($n = 2$) 3D NMR pulse sequences for measuring C2′, C3′, and C4′ chemical shifts in RNA. (B) Straight-through (H5)C5(C4C3C2)C1H1 3D NMR pulse sequence for measuring C5′ chemical shifts in RNA. For both panels: narrow bars and wide bars correspond to 90° and 180° pulses, respectively; pulses have phase x unless otherwise noted; ^{15}N decoupling was applied during the t_2 evolution period (not shown); delay durations are given by $\Delta = 1/(2J_{CH})$ and $\tau = 1/(4J_{CC}) = 6.25$ ms; the cryogenic probe used at 18.8 T allowed only z-axis pulsed field gradients. For part (A): a shaped 180° reBURP pulse[51] of length 2.7 ms (at 18.8 T) and centered on H1′ was applied; phase cycling is as follows: $\phi_1 = y, -y; \phi_2 = -y; \phi_3 = y, y, -y, -y; \phi_4 = x; \phi_5 = x, -x, \phi_{rec} = x, -x, -x, x$; quadrature detection in the t_1 dimension was achieved by simultaneously incrementing ϕ_1, ϕ_2, and ϕ_4 in the regular States-TPPI manner; quadrature detection in the t_2 dimension was achieved by simultaneously inverting the polarity of gradients G3 and G4, as well as the phase of the subsequent 90° [13]C pulse; the ^{13}C carrier was placed at 82 ppm, and the F_1 and F_2 frequencies were aliased into a ∼5 ppm window; pulsed field gradients sine-bell shaped with durations of: $G_{0,1,2,3,4,5,6,7,8}$ = 300, 400, 250, 1000, 1000, 267, 300, 201.5, 301.5 μs and with peak amplitudes of $G_{0,1,2,3,4,5,6,7,8}$ = 24, 24, 15, 33, −27, 31, 14, 30, −30 G/cm. For part (B): a shaped 180° iBURP pulse[51] of length 2.0 ms (at 18.8 T), centered at 62.7 ppm, was applied; a [1]H 90° pulse is applied after t_1 to eliminate unwanted coherences; phase cycling is as follows: $\phi_1 = x, -x; \phi_{rec} = x, -x$; quadrature detection in the t_1 dimension was achieved by incrementing ϕ_1 in the regular States-TPPI manner; quadrature detection in the t_2 dimension was achieved by simultaneously inverting the polarity of gradients G5 and G6, as well as the phase of the subsequent 90° [13]C pulse; the ^{13}C carrier was placed at 82 ppm and the F_1 and F_2 frequencies were aliased into a ∼5 ppm window; pulsed field gradients are sine-bell shaped with durations of: $G_{0,1,2,3,4,5,6,7,8,9,10}$ = 300, 250, 400, 100, 200, 1000, 1000, 267, 300, 201.5, 301.5 μs and with peak amplitudes of $G_{0,1,2,3,4,5,6,7,8,9,10}$ = 24, 16, 4, 24, 20, 33, −27, 19, 14, 30, −30 G/cm. Code and parameters used for implementation on Bruker Avance equipment are available at http://spin.niddk.nih.gov/bax/.

$1/J_{CC}$ constant-time t_1 interval of 25 ms on either C2′, C3′, or C4′. The magnetization is then transferred back to C1′ for a second constant-time interval of 34.4 ms ($3/2J_{CC}$), corresponding to t_2 evolution, prior to detection on H1′ during t_3. These experiments also provided additional replicate $\Delta\delta$(C1′) measurements in their F_2 dimensions. Values of $\Delta\delta$([13]C5′) were measured using the "straight-through" (H5)C5(C4C3C2)C1H1 sequence of Figure 2B. We note that these pulse sequences, when implemented without ^{1}H decoupling in the indirect dimensions, also provide efficient new methods of obtaining one-bond [13]C−[1]H RDCs.

Presented in Figure 3 are selected 2D planes taken from the 3D H1C1C2, H1C1(C2)C3, H1C1(C2C3)C4, and (H5)C5-(C4C3C2)C1H1 spectra, which depict the chemical shifts observed in isotropic and aligned samples. For example, large negative $\Delta\delta$ are observed for C3′ (−55 ppb) and C4′ (−59 ppb) of cytidine 59 while a positive $\Delta\delta$ of 35 ppb is observed for C5′ of the same nucleotide. Cytidine C40 clearly exhibits smaller values of $\Delta\delta$ in all three cases. Anisotropic C1′ shifts may be extracted from the orthogonal dimension of each 3D spectrum; clearly from these slices, both δ_{iso} and δ_{aniso} from C1′ are reproducible in the different experiments.

For all experiments, the $\Delta\delta$(H1′) data served as an important internal calibration, as these values must be no more than a few ppb considering the small value of aliphatic ^{1}H chemical shift anisotropy. Larger differences, as observed for loop residues (data not shown), are indicative of minute shifts in the multiconformer equilibrium of the flexible loop structure, presumably resulting from the presence of Pf1. Data for the last stem basepair, U44-A53 were also among those affected, with an exceptionally large $\Delta\delta$(H1′) for U44 (−14 ppb), and a very weak resonance for A53. Data for the other terminal basepair, G37-C60, also were excluded since previous work[45] has shown this basepair to be subject to rapid internal dynamics of substantial amplitude, which would scale the apparent CS tensor parameters.

Determination of Chemical Shift Tensors. Having measured a complete set of anisotropic shifts, SVD fits of these data to various RNA structures were carried out in the manner described below, to determine CS tensor magnitudes and orientations. SVD fitting is a reliable and commonly used method for determining molecular alignment tensor parameters on the basis of a known structure and a set of RDCs.[46,47] The structure of the A-form stem of helix-35ψ RNA has been refined, starting

Table 1. Measured Anisotropic Chemical Shifts[a] (in ppb) for the Ribose Carbons of the A-Form Helical Stem of Helix-35ψ RNA[b,c]

	C1′	C2′	C3′	C4′	C5′
G38	6.6	6.0	−42.5	−56	−12
G39	5.4	7.5	−28.0	−35	−4
C40	2.6	2.0	−9.5	−18	−11
U41	1.1	−5.0	−14.0	−16	−3
A42	4.9	1.5	−24.0	−19	3
A43	−4.5	−0.5	−30.0	−40	16
U54	−1.2	6.0	−24.0	−33	−14
U55	−6.2	0.0	−31.5	−30	4
A56	−1.7	−3.0	−44.5	−34	11
G57	−1.6	−4.0	−57.5	−58	6
C58	−5.1	−4.5	−58.5	−64	19
C59	−6.2	2.0	−56.0	−65	35
C60	4.6	−2.0	−39.0	−52	29
estimated error	±1.4	±3.3	±2.4	±9[d]	±8

[a] Values shown are $\Delta\delta = \delta_{aniso} - \delta_{iso}$, where δ_{aniso} is the apparent chemical shift measured on the Pf1-aligned sample and δ_{iso} is the chemical shift measured on the isotropic sample. [b] Data for C60 were excluded due to large amplitude internal dynamics of this residue. Data for U44 were excluded from all fits due to unacceptably large values of $\Delta\delta$(H1′) (−14 ppb). Resonances for A53 were generally too weak to be observed. Nucleotide G37 was not ^{13}C-enriched. [c] Data for C1′ result from averaging data measured from 2CT-HSQC-RK experiments at 750 and 800 MHz, a 2CT-HSQC-WG experiment at 800 MHz, and 3D H1C1C2 and H1C1(C2)C3 experiments at 800 MHz. Numbers reported for C2′ are the average of data obtained from 3D H1C1C2 datasets obtained at 750 and 800 MHz. Numbers reported for C3′ are the average of data obtained from 3D H1C1(C2)C3 datasets obtained at 750 and 800 MHz. Numbers reported for C4′ are the average of data obtained from 3D H1C1(C2C3)C4 datasets obtained at 750 and 800 MHz. Numbers reported for C5′ are the average of data obtained from two independent 3D (H5)C5(C4C2C2)C1H1 datasets obtained at 800 MHz. [d] The rmsd is dominated by two points (A42 and A56).

from a canonical A-form helix, by using a large number of ^{13}C−^{1}H, ^{1}H−^{1}H, ^{13}C−^{13}C, and ^{13}C−^{15}N RDC restraints, anisotropic ^{31}P chemical shifts, and torsion angle restraints from J couplings. The molecular alignment tensor magnitude and rhombicity, $D_a{}^{CH} = -28.9$ Hz and $R = 0.26$, and its orientation with respect to the molecular framework are necessary for the determination of the ribose carbon CS tensors. The principal components of the alignment tensor are: $A_{ZZ} = 8.26 \times 10^{-4}$, $A_{YY} = -5.74 \times 10^{-4}$, $A_{XX} = -2.52 \times 10^{-4}$, where the *capitalized* subscripts refer to the principal axis system (PAS) of the alignment tensor. The procedure used in the SVD fitting of anisotropic shifts will be described for the case of C1′ (Figure 1C), but is of course fully analogous for all other carbons.

The traceless symmetric part of the CS tensor for a given nucleus is described by a 3×3 matrix consisting of up to five independent components:

$$\boldsymbol{\delta}^{sym} = \begin{bmatrix} \delta_{xx} & \delta_{xy} = \delta_{yx} & \delta_{xz} = \delta_{zx} \\ \delta_{yx} = \delta_{xy} & \delta_{yy} & \delta_{yz} = \delta_{zy} \\ \delta_{zx} = \delta_{xz} & \delta_{zy} = \delta_{yz} & \delta_{zz} \end{bmatrix} \quad (2)$$

Here, we neglect the antisymmetric portion of $\boldsymbol{\delta}$ and have subtracted the isotropic contribution, δ_{iso}. Upon diagonalization of $\boldsymbol{\delta}^{sym}$, three principal components (δ_{11}, δ_{22}, and δ_{33}) and three angles relating the PAS of $\boldsymbol{\delta}^{sym}$ to the molecular framework are obtained. Since we are considering the traceless part of $\boldsymbol{\delta}$, only two of the three principal components are independent.

A fundamental assumption in our analysis is that, due to the well-characterized uniformity of A-form RNA, all the stem nucleotide C1′ nuclei may be described by a single CS tensor of uniform magnitude and orientation with respect to the *local*

molecular framework. The fact that all ^{13}C1′ nuclei of the A-form helical stem resonate within the narrow range of 93.3 ± 1 ppm is consistent with the assumption of an essentially uniform CS tensor. For C1′, we define this local axis system such that the x-axis bisects the O4′−C1′−C2′ angle, the y-axis lies in the same plane and perpendicular to x, and the z-axis is perpendicular to the plane. The next step is to express the molecular alignment tensor in the local xyz axis system of each C1′. We denote the five independent components of the traceless alignment tensor in this frame as $A_{yy}-A_{xx}$, $A_{zz}-A_{xx}$, $2A_{xy}$, $2A_{xz}$, $2A_{yz}$, where the *lowercase* subscripts refer to the local C1′ axis system. Note that these components will therefore be different for each C1′. Equation 1 then may be expanded and re-expressed as a matrix equation as follows:

$$\begin{bmatrix} A_{yy}^{(1)} - A_{xx}^{(1)} & A_{zz}^{(1)} - A_{xx}^{(1)} & 2A_{xy}^{(1)} & 2A_{xz}^{(1)} & 2A_{yz}^{(1)} \\ A_{yy}^{(2)} - A_{xx}^{(2)} & A_{zz}^{(2)} - A_{xx}^{(2)} & 2A_{xy}^{(2)} & 2A_{xz}^{(2)} & 2A_{yz}^{(2)} \\ \vdots & \vdots & \vdots & \vdots & \vdots \\ \vdots & \vdots & \vdots & \vdots & \vdots \\ \vdots & \vdots & \vdots & \vdots & \vdots \\ A_{yy}^{(N)} - A_{xx}^{(N)} & A_{zz}^{(N)} - A_{xx}^{(N)} & 2A_{xy}^{(N)} & 2A_{xz}^{(N)} & 2A_{yz}^{(N)} \end{bmatrix} \begin{bmatrix} \delta_{yy} \\ \delta_{zz} \\ \delta_{xy} \\ \delta_{xz} \\ \delta_{yz} \end{bmatrix}$$

$$= \begin{bmatrix} \Delta\delta^{(1)} \\ \Delta\delta^{(2)} \\ \vdots \\ \vdots \\ \Delta\delta^{(N)} \end{bmatrix} \quad (3)$$

where each row of the $5 \times N$ matrix and each row of the $1 \times N$ matrix correspond to a given nucleotide's C1′ nucleus, where N is the total number of datapoints/nucleotides being considered (12 in our case). The 1×5 column vector contains the five independent elements of the traceless symmetric CS tensor. A singular-value decomposition of the $5 \times N$ matrix may now be applied to determine the five components of the CS tensor. Finally, a 3×3 symmetric matrix is constructed from these components (eq 2) and diagonalized to yield the principal components of the traceless part of the CS tensor and its orientation with respect to the local C1′ xyz axis system. The same procedure is subsequently carried out independently for C2′, C3′, C4′, and C5′ nuclei. The CS tensor results are reported in Tables 2 and 3.

Fits to a Database of RNA X-ray Structures. Results of the above-described fitting procedure are very sensitive to minor variations in the structure. It is well-recognized that an ensemble of dipolar-refined structures generally underestimates the experimental uncertainty in such structures.[60] Therefore, in addition to fitting the measured $\Delta\delta$ to the NMR-refined structure of helix-35ψ RNA, an automated systematic search of the Protein Databank[61] for high-resolution X-ray structures of RNA containing segments of at least six consecutive canonical Watson−Crick base pairs was carried out. For each six-basepair database "hit", a set of 60 one-bond ^{13}C−^{1}H and three-bond ^{1}H−^{1}H RDCs ($^1D_{C1'H1'}$, $^1D_{C2'H2'}$, $^1D_{C3'H3'}$, $^1D_{C4'H4'}$, $^3D_{H1'H2'}$) measured

(60) Tjandra, N.; Tate, S.; Ono, A.; Kainosho, M.; Bax, A. *J. Am. Chem. Soc.* **2000**, *122*, 6190−6200.
(61) Berman, H. M.; Westbrook, J.; Feng, Z.; Gilliland, G.; Bhat, T. N.; Weissig, H.; Shindyalov, I. N.; Bourne, P. E. *Nucleic Acids Res.* **2000**, *28*, 235−242.
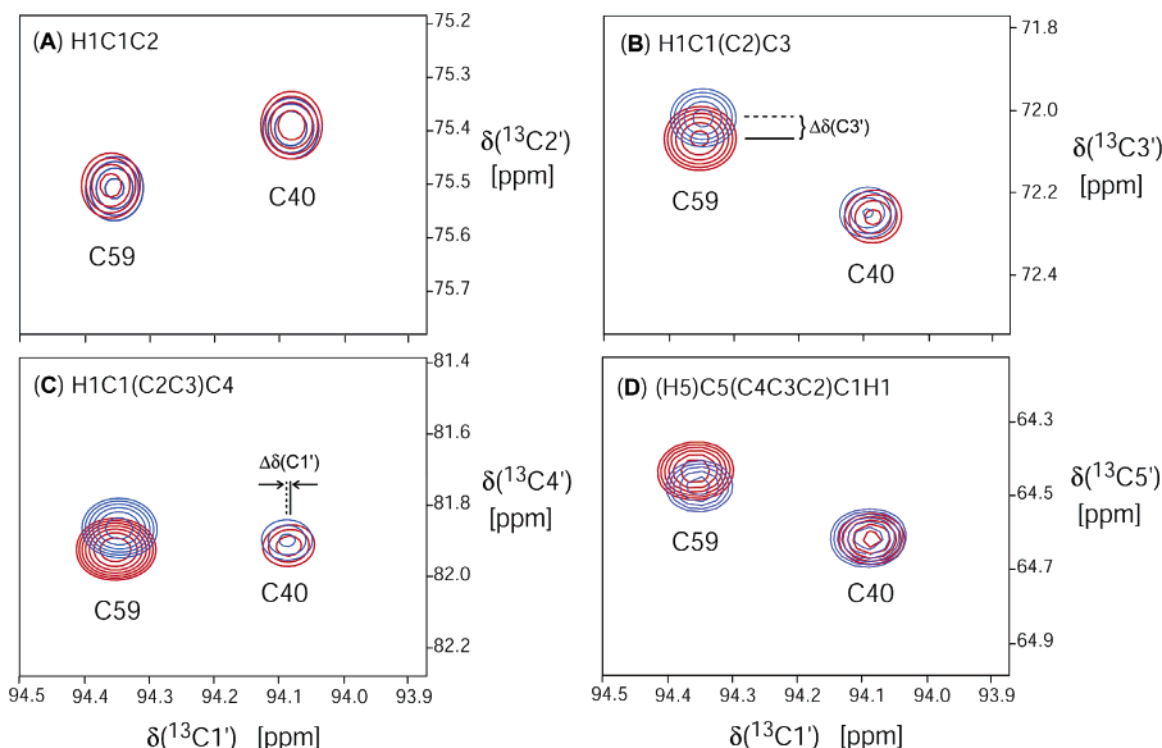
Figure 3. Selected 2D planes from the (A) H1C1C2, (B) H1C1(C2)C3, and (C) H1C1(C2C3)C4, (D) (H5)C5(C4C3C2)C1H1 3D NMR spectra, recorded for helix-35ψ RNA at 800 MHz. Red contours correspond to the isotropic sample, blue to the aligned sample. All four planes correspond to the same ^{1}H chemical shift of 5.50 ppm.

Table 2. Summary of Average Ribose Carbon Chemical Shift Tensor Magnitudes[a] Determined for the Helical Stem Residues of Helix-35ψ RNA

atom	structure or method	δ_{11}/ppm	δ_{22}/ppm	δ_{33}/ppm	rmsd (fit)/ppb	rmsd (xval)/ppb	Q_{fit}[b]/%	Q_{xval}[c]/%
C1′	NMR-refined: fit	17.7 ± 0.2	−0.89 ± 0.03	−16.8 ± 0.2	2.25		17.7	
	NMR-refined: xval	17.6 ± 1.6	−0.88 ± 0.59	−16.6 ± 1.6		3.64		28.7
	database[d](fit)	14.8 ± 3.9	−0.1 ± 0.7	−14.9 ± 4.2	2.18	3.78	19.8	34.3
	RHF[e]	16.4	1.4	−17.8	−	−	−	−
	DFT[f]	17.7	3.7	−21.4	−	−	−	−
C2′	NMR-refined: fit	12.8 ± 0.1	1.0 ± 0.1	−13.8 ± 0.1	2.27		23.3	
	NMR-refined: xval	13.0 ± 1.3	1.0 ± 0.7	−14.0 ± 0.9		3.59		36.9
	database (fit)	12.3 ± 1.9	1.1 ± 0.4	−13.3 ± 1.8	1.93	3.35	20.6	35.8
	RHF	10.8	6.6	−17.4	−	−	−	−
	DFT	11.2	6.5	−17.7	−	−	−	−
C3′	NMR-refined: fit	45.7 ± 0.3	4.2 ± 0.3	−49.9 ± 0.2	3.60		10.3	
	NMR-refined: xval	46.1 ± 2.2	3.8 ± 3.2	−50.0 ± 1.6		6.68		19.1
	database (fit)	34.4 ± 7.4	12.8 ± 5.5	−47.3 ± 2.9	8.05	13.8	27.3	46.8
	RHF	26.2	8.4	−34.5	−	−	−	−
	DFT	29.4	7.5	−36.9	−	−	−	−
C4′	NMR-refined: fit	44.8 ± 0.3	2.1 ± 0.3	−46.9 ± 0.1	3.40		10.1	
	NMR-refined: xval	45.1 ± 1.9	1.8 ± 2.7	−46.9 ± 1.4		6.14		18.2
	database (fit)	47.5 ± 7.9	3.3 ± 8.7	−50.8 ± 3.0	5.32	9.01	14.8	25.0
	RHF	34.2	3.7	−37.9	−	−	−	−
	DFT	37.4	5.5	−42.9	−	−	−	−
C5′	NMR-refined: fit	19.4 ± 0.2	17.5 ± 0.1	−37.0 ± 0.2	7.60		35.9	
	NMR-refined: xval	21.5 ± 4.4	15.0 ± 4.4	−36.5 ± 6.3		13.8		65.1
	database (fit)	27.4 ± 9.6	7.6 ± 4.7	−35.0 ± 10.0	7.53	14.7	33.5	65.3
	RHF	21.2	10.5	−31.6	−	−	−	−
	DFT	27.6	12.4	−40.0	−	−	−	−

[a] The principal components are ordered $\delta_{11} \geq \delta_{22} \geq \delta_{33}$, and refer to the traceless symmetric part of the chemical shift tensor. [b] Q_{fit} is the quality factor of the fitted anisotropic shifts (see eq 4). [c] Q_{xval} is the free quality factor resulting from independent cross-validation of each experimental data point. [d] Database statistics are based on the following quality cutoffs: rmsd fit of $^1D_{CH}$ RDCs to structure below 4.0 Hz; X-ray resolution below 2.5 A. [e] RHF/cc-pVTZ results for a guanidine nucleotide. See Experimental Section and Supporting Information for further details and additional results. [f] B3LYP/cc-pVTZ results for a guanidine nucleotide.

for the ribose moieties of helix-35ψ RNA was SVD-fitted to the structure. Base couplings were not used in this process because the types of nucleotides generally did not match those of the helix-35 stem region. The fitted alignment tensor was then used in combination with the structure and experimental

$\Delta\delta$ values to SVD-fit the CS tensor (cf. eq 3). Results are given in Tables 2 and 4. To guard against the fact that the SVD method always yields an answer, regardless of the quality of the input data, results were filtered according to the following criteria chosen to obtain a subset of the 10−20 highest-quality CS

Table 3. Experimental Average Ribose Carbon Chemical Shift Tensor Orientations Determined for the A-Helical Stem Residues of Helix-35ψ RNA (expressed as direction cosines)[a] for the NMR-Refined Structures[b]

nucleus		x[c]	y	z
C1′	δ_{11}	0.00	0.07	−1.00
		0.00 ± 0.04	0.07 ± 0.02	−1.00 ± 0.01
	δ_{22}	0.977	−0.21	−0.01
		0.98 ± 0.01	−0.21 ± 0.03	−0.01 ± 0.04
	δ_{33}	0.212	0.97	0.06
		0.21 ± 0.04	0.97 ± 0.01	0.06 ± 0.03
C2′	δ_{11}	0.76	0.32	−0.57
		0.75 ± 0.05	0.31 ± 0.06	−0.58 ± 0.08
	δ_{22}	0.022	0.86	0.51
		0.03 ± 0.10	0.87 ± 0.01	0.49 ± 0.03
	δ_{33}	0.65	−0.40	0.65
		0.65 ± 0.04	−0.39 ± 0.04	0.65 ± 0.06
C3′	δ_{11}	−0.57	−0.05	0.82
		−0.57 ± 0.01	−0.06 ± 0.09	0.82 ± 0.02
	δ_{22}	−0.03	1.00	0.04
		−0.04 ± 0.05	0.99 ± 0.01	0.04 ± 0.08
	δ_{33}	−0.82	0.00	−0.57
		−0.82 ± 0.01	0.00 ± 0.02	−0.57 ± 0.01
C4′	δ_{11}	0.099	0.12	0.99
		0.09 ± 0.11	0.13 ± 0.07	0.98 ± 0.02
	δ_{22}	−0.88	0.47	0.03
		−0.73 ± 0.48	0.40 ± 0.23	0.07 ± 0.11
	δ_{33}	−0.46	−0.87	0.15
		−0.46 ± 0.01	−0.87 ± 0.01	0.15 ± 0.02
C5′	δ_{11}	−0.87	−0.46	−0.11
		−0.53 ± 0.49	−0.35 ± 0.17	0.23 ± 0.51
	δ_{22}	−0.07	−0.10	0.99
		−0.396 ± 0.300	−0.23 ± 0.17	0.21 ± 0.79
	δ_{33}	0.47	−0.88	−0.06
		0.46 ± 0.10	−0.88 ± 0.05	−0.07 ± 0.05

[a] The principal components are ordered $\delta_{11} \geq \delta_{22} \geq \delta_{33}$, and refer to the traceless symmetric part of the chemical shift tensor. [b] The first row of each entry is the average value resulting from direct fits using all data points. The second row is the average and standard deviation resulting from cross-validation of each experimental CSA data point. [c] The xyz axis systems used are defined as follows. C1′: x bisects the O4′−C1′−C2′ angle, y is in the same plane, z is perpendicular to this plane (see Figure 1C); C2′: x bisects the C1′−C2′−C3′ angle, y is in the same plane, z is perpendicular to this plane; C3′: x bisects the C2′−C3′−C4′ angle, y is in the same plane, z is perpendicular to this plane; C4′: x bisects the C3′−C4′−O4′ angle, y is in the same plane, z is perpendicular to this plane; C5′: x bisects the O5′−C5′−C4′ angle, y is in the same plane, z is perpendicular to this plane.

Table 4. Experimental Average Ribose Carbon Chemical Shift Tensor Orientations Determined for the A-Helical Stem Residues of Helix-35ψ RNA (expressed as direction cosines): Fits to X-ray Database[a,b]

nucleus		x	y	z
C1′	δ_{11}	−0.13 ± 0.12	−0.09 ± 0.06	−0.98 ± 0.02
	δ_{22}	−0.98 ± 0.02	0.07 ± 0.10	0.12 ± 0.11
	δ_{33}	0.05 ± 0.09	0.99 ± 0.01	−0.11 ± 0.06
C2′	δ_{11}	0.76 ± 0.04	0.36 ± 0.10	−0.51 ± 0.11
	δ_{22}	−0.08 ± 0.12	0.86 ± 0.06	0.48 ± 0.07
	δ_{33}	0.62 ± 0.06	−0.34 ± 0.03	0.70 ± 0.06
C3′	δ_{11}	0.50 ± 0.16	0.11 ± 0.60	−0.56 ± 0.20
	δ_{22}	−0.08 ± 0.40	0.75 ± 0.25	0.08 ± 0.45
	δ_{33}	0.75 ± 0.02	0.00 ± 0.06	0.66 ± 0.02
C4′	δ_{11}	−0.11 ± 0.31	−0.06 ± 0.20	−0.91 ± 0.11
	δ_{22}	0.79 ± 0.09	−0.47 ± 0.07	−0.06 ± 0.37
	δ_{33}	−0.50 ± 0.05	−0.85 ± 0.03	0.10 ± 0.03
C5′	δ_{11}	0.28 ± 0.49	0.36 ± 0.27	−0.52 ± 0.46
	δ_{22}	0.48 ± 0.55	0.11 ± 0.24	0.45 ± 0.44
	δ_{33}	0.30 ± 0.24	−0.85 ± 0.13	−0.34 ± 0.06

[a] See footnotes to Table 3 for additional details. [b] Results have been filtered according to criterion of footnote d in Table 2.

tensors: resolution of X-ray structure (below 2.5 Å); rmsd of initial fit of RDCs to the structure (<4 Hz).

Quality of Fit and Cross-Validation of Chemical Shift Tensors. Here, we evaluate the quality of $\Delta\delta$ data predicted from the CS tensor solution, and how the predicted values compare with the experimental $\Delta\delta$ data. Shown in Figure 4 are plots of the fitted $\Delta\delta$ (filled circles) against the experimental $\Delta\delta$ data for C1′, C2′, C3′, C4′, and C5′. The highest correlations are observed for C3′ and C4′, due to the large range of the data as well as the large magnitude of many of the experimental $\Delta\delta$ points compared to the measurement error. Owing to the much smaller range of $\Delta\delta$ measured for C1′ and C2′, visually these data do not appear as strongly correlated. However, $\Delta\delta$ for C1′ and C2′ are actually fit with lower root-mean-square (rms) devations (2.25 and 2.27 ppb) than those for C3′ and C4′ (see Table 2). Furthermore, the fitted Q-factors for all four types of carbons are comparable (Table 2), where Q is defined as:

$$Q = \frac{\text{rms}(\Delta\delta_{\text{expt}} - \Delta\delta_{\text{pred}})}{\sqrt{\left(\delta_a^2\left(1 + \frac{\eta^2}{3}\right)\right)\left(\frac{4 + 3R^2}{5}\right)}} \qquad (4)$$

Here, $\Delta\delta_{\text{pred}}$ refers to predicted values of $\Delta\delta$, resulting from the SVD fit. The quantity δ_a is equal to one-half of the largest possible anisotropic shift $\Delta\delta$ determined from the SVD fit, assuming a uniform distribution of CS tensors with respect to the molecular alignment tensor. R is the rhombicity of the alignment tensor. The asymmetry of the traceless part of the chemical shift tensor, η, is defined as $(\delta_{xx} - \delta_{yy})/\delta_{zz}$, where $|\delta_{zz}| \geq |\delta_{yy}| \geq |\delta_{xx}|$.

To further assess the quality of the results, we have cross-validated each data point by performing an SVD fit using only 11 data points, and then using the resulting CS tensor components to predict $\Delta\delta$ for the 12th point. This procedure is repeated 12 times, once for each data point. The predicted $\Delta\delta$'s resulting from this procedure are plotted as open circles in Figure 4. This cross-validation of the results is somewhat stringent since we are excluding over 8% of the experimental data in each cross-validation, and as a result our ratio of data to unknowns is only 2.2. Nevertheless, the cross-validation statistics (Table 2) for C1′, C2′, C3′, and C4′ are very good, with C4′ showing the best results with a cross-validated Q-factor of 18% for the NMR structure. Also shown in Table 2 are the average chemical shift tensor principal components and their associated standard deviations resulting from the cross-validation procedure. To further assess the precision of the results, random noise was added to the CSA data (50000 replicates per structure; 10 NMR structures) at the level of the experimental rmsd, and SVD fits were carried out (see Table 6S, Supporting Information).

For C1′, C2′, and C5′ the quality of fits to the best database structures are comparable with the quality of fits obtained with the NMR-refined structures (Table 2); however, the reported principal components are necessarily less precise for the database of X-ray structures considering the substantial structural variation (mean pairwise rmsd of 0.73 Å over the ribose heavy atoms) among the database structures used. For C3′ and, to a lesser extent for C4′, the NMR-refined structures cross validate considerably better than the structures extracted from the database.

The fit and cross-validation statistics for C5′ (Table 2) are poorer than for the ring carbons. This is true both of fits to the NMR-refined helix as well as fits to the X-ray database,
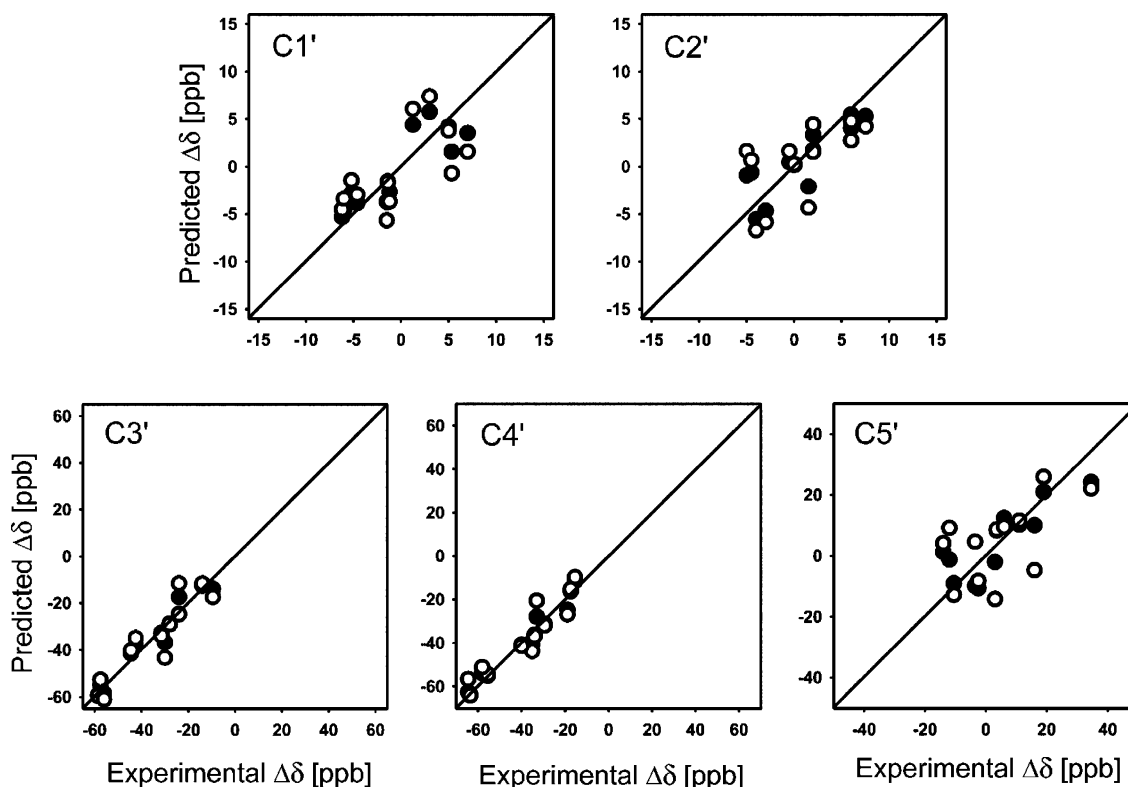
Figure 4. Correlation between experimental and predicted values of $\Delta\delta$ for the ribose carbon atoms, C1′, C2′, C3′, C4′, and C5′. Predicted values are averages over an ensemble of 25 NMR-refined structures of helix-35ψ RNA. Closed circles represent the predicted values resulting from an SVD fit of the 12 experimental data points to the refined A-form helical segment of helix-35ψ RNA. Open circles represent the predicted values resulting from cross-validation. The cross-validated points are obtained by SVD-fitting 11 data points to the NMR structures and using the CS tensor resulting from the fit to independently predict the remaining 12th point and repeating this procedure 12 times. Data are plotted over the approximate maximum range of $\Delta\delta$ expected if the ribose moieties were uniformly distributed relative to the alignment tensor, as determined from the SVD fit. Fit statistics are given in Table 2.

suggesting that there is no deficiency specific to either the NMR or X-ray structures around C5′. In addition to the relatively high experimental rmsd in the measured anisotropic shifts for C5′ (Table 1), the wide spread in the magnitude and orientations resulting from fits to the X-ray database indicates that the outcome is exceptionally sensitive to the precise geometry of this methylene group relative to the alignment tensor. As judged by fits to the database, the lack of precision of the C5′ results may arise from poorly defined orientations of the two least shielded components of the CS tensor, despite the fact that the quantum chemical results indicate a considerable degree of asymmetry of this chemical shift tensor ($\eta = 0.37$) (Table 2 and Supporting Information).

The residual rmsds in the fits for all carbons reflect both the assumption of a uniform CS tensor for all nuclei of a given type as well as errors in the experimental $\Delta\delta$ values and experimental uncertainties in the NMR and X-ray structures. However, the nonrandom distribution of the ribose orientations relative to the molecular alignment tensor causes structural and measurement errors to propagate differently for different nuclei when deriving the CS tensors.

Tensor Magnitudes and Orientations. The tensor spans ($\Omega = \delta_{11} - \delta_{33}$) resulting from fits to the NMR-refined RNA structure range from 27 ppm for C2′ to 96 ppm for C3′ (Table 2 and Figure 5). While it is difficult to quantitatively explain the relative magnitudes of the spans for the five types of carbons, we note that C3′ and C4′, which exhibit the largest spans, also exhibit the largest rms deviation of their surrounding six covalent bond angles from the ideal tetrahedral angle of 109.47° (4.1

and 4.4°, respectively). It is apparent, however, that there is no single dominant geometrical factor that exclusively determines the magnitude of the CSA for the different types of ribose carbons. In the present case, no simple correlation is expected to be perfect for several reasons, including the fact that different substituent atoms with different bond lengths are present on the different carbons.

The measured span for C1′, 35 ppm, is in good agreement with the value measured for a powdered sample of adenosine (33 ppm) by FIREMAT solid-state NMR.[43] However, the range of C1′ values for isolated nucleotides reported by Stueber and Grant extends from 33 ppm for adenosine, 36 ppm for cytidine, 58 ppm in guanosine dihydrate, to a maximum of 75 ppm for 2′-deoxythymidine. This wide range of values underscores the need to determine the tensors on an oligonucleotide of relevant conformation in solution, if the tensors are to be used successfully as structural restraints in future studies of RNA in solution. In addition to the earlier solid-state NMR studies of powdered samples, our studies now also define the required orientation of the CS tensor with respect to the molecular framework.

Results from RHF and DFT calculations of the ribose carbon CS tensors (Table 2 and Supporting Information) are generally in reasonable agreement with the experimental results (see Figure 5). The trends in anisotropy and asymmetry of the tensors are well reproduced. For all carbons, the DFT results predict a larger magnitude for δ_{33} than do the RHF calculations. For C1′ and C5′, this results in a notably better agreement with experiment for the RHF calculations than for the DFT calculations; however, for other carbons it is clear that the DFT results
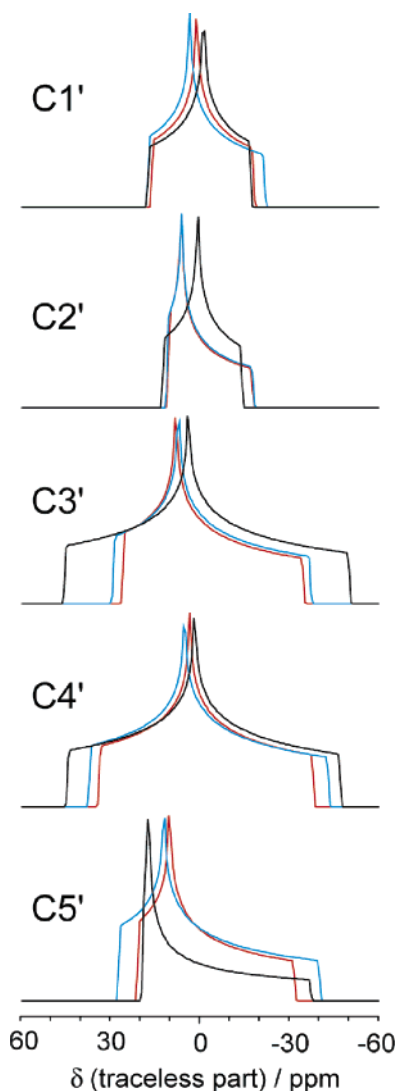
Figure 5. Comparison between simulated chemical shift powder patterns generated from experimental (fit to the NMR structure of helix-35ψ RNA in black) and theoretical (B3LYP/cc-pVTZ in blue; RHF/cc-pVTZ in red) principal components. Note that only the traceless portion of the CS tensors has been plotted, to facilitate comparison between the different carbons. The figures were generated using WSOLIDS.[62]
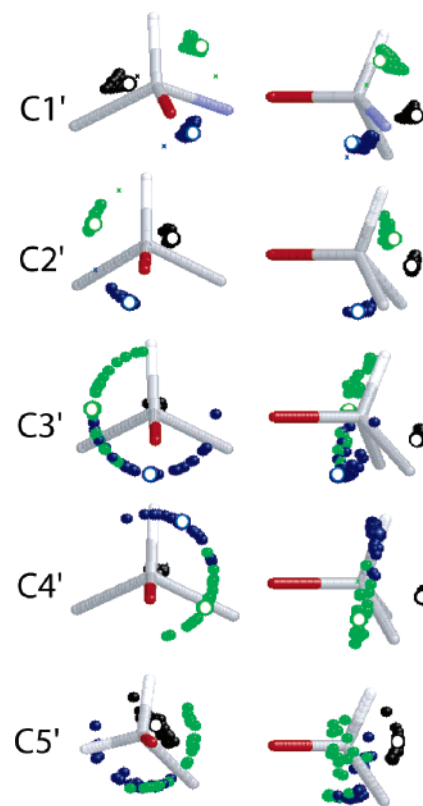

Figure 6. Experimental and DFT-calculated (B3LYP/6-311+G*) CS tensor orientations for the ribose carbon nuclei. Two views are shown for each type of carbon, for clarity. Hollow circles depict the experimental orientations from fits to the NMR structure of helix-35ψ RNA; filled circles represent the fit to a database of high-resolution X-ray structures; small crosses represent the DFT orientations. For C5′, the nearly axially symmetric tensor obtained from fits to the NMR structures result in undefined orientations of the δ_{11} and δ_{22} axes. The most shielded component, δ_{33}, is shown in black, δ_{22} in green, δ_{11} in blue. In several instances, the DFT orientations fall within the experimental range, and the crosses are not visible. The tensor components are not always depicted in a right-handed fashion in the presentation of the results. The atoms shown for the C1′ frame are: O4′, C2′, N9, H1′; for C2′: C1′, C3′, O2′, H2′; for C3′: O3′, C2′, C4′, H3′; for C4′: C3′, C5′, O4′, H4′; for C5′: C4′, O5′, H5′, H5″. Oxygen atoms are shown in red; carbons in gray; hydrogens in white, nitrogen in blue.

are closer to experiment. The orientations of the tensors predicted by the two methods are consistent to within a few degrees.

The calculations consistently correctly predict the experimentally determined direction of the most shielded component, δ_{33}, to within a few degrees (Table 6S and Figure 6). We find that, for all types of carbons, this component lies approximately along the local carbon−oxygen bond axis. This is in direct contrast with the situation for carbonyl carbons, for which δ_{33} lies perpendicular to the plane containing the C=O bond.[63−65] The differences in orientation, as well as span, of the CS tensors for ribose and carbonyl carbons arise from the differences in

electronic structure surrounding these nuclei, particularly the lack of the appropriate magnetic-dipole-allowed transitions which are known to be largely responsible for the ^{13}C carbonyl CS tensor properties.[65,66]

Also shown in Figure 6 are the tensor orientations resulting from the database fits. While there is considerable variability in these orientations, their averaged orientations generally agree with those obtained from fits to the NMR structures. The database results also consistently indicate that δ_{33} is aligned approximately along the local C−O bond axis.

The good agreement between experiment and theory is despite the fact that the calculations are carried out on isolated molecules in vacuo, without explicit consideration of solvation or surrounding charged ions or of adjacent nucleotides. Furthermore, the experimental result is effectively an average over the geometries of the 12 nucleotides and their CS tensors, while the calculated results are for a single, fixed geometry. Clearly, the CS tensors are expected to be sensitive to the torsion angles defining the geometry of the nucleotide. Previous experimental

(62) Eichele, K.; Wasylishen, R. E. *WSOLIDS1 NMR Simulation Package,* Version 1.17.30; University of Tubingen (http://casgm3.anorg.chemie. uni-tuebingen.de/klaus/soft/index.html), 2001.
(63) Stark, R. E.; Jelinski, L. W.; Ruben, D. J.; Torchia, D. A.; Griffin, R. G. *J. Magn. Reson* **1983**, *55*, 266−273.
(64) Teng, Q.; Iqbal, M.; Cross, T. A. *J. Am. Chem. Soc.* **1992**, *114*, 5312−5321.
(65) Lumsden, M. D.; Wasylishen, R. E.; Eichele, K.; Schindler, M.; Penner, G. H.; Power, W. P.; Curtis, R. D. *J. Am. Chem. Soc.* **1994**, *116*, 1403−1413.

(66) Schindler, M.; Kutzelnigg, W. *J. Chem. Phys.* **1982**, *76*, 1919−1933.

and theoretical results have demonstrated the sensitivity of the ^{13}C chemical shift and/or chemical shift anisotropy to nucleotide conformation.[67−70] A more quantitative agreement with experiment may be possible by explicitly considering the influence of dynamics, solvation, and/or long-range electrostatic effects. However, even in this case one may reach the limits on agreement imposed by the assumption of a uniform tensor. Indeed, a notable improvement in the agreement between experimental and predicted $\Delta\delta$ for ubiquitin was obtained by Markwick and Sattler[37] through the implementation of a combined molecular dynamics and DFT study which allows for site-specific CS tensors.

Concluding Remarks

The magnitude and orientations of the five ribose carbon CS tensors have been characterized by liquid crystal NMR spectroscopy, thereby providing new opportunities for RNA structure refinements based on anisotropic chemical shift measurements. The relative simplicity of the pulse sequences used, as well as the relative ease with which measurements and data analysis are carried out, implies that anisotropic shift measurements may become an important and valuable piece of information for structural refinements of RNA, as has been previously demonstrated for proteins. In this respect, our results indicate that $\Delta\delta(^{13}\mathrm{C3}')$ and $\Delta\delta(^{13}\mathrm{C4}')$ will provide the most robust information, which may be particularly useful when working with oligonucleotides that are selectively deuterated for improving ^{1}H relaxation properties,[71] for which the number of accessible $^{1}D_{\mathrm{CH}}$ couplings is very small.

Our analysis is based on the premise that the ribose ^{13}C CS tensor is independent of the type of nucleotide. This premise is reasonable, as it is known that isotropic ^{13}C ribose chemical shifts depend primarily on ring pucker and not on nucleotide type.[68,72] Invariance of the ribose ^{13}C CS tensor between pyrimidine and purine nucleotides is also supported by quantum chemical calculations, which show only minute effects of the base substitutions on the computed ribose ^{13}C CS tensors (data not shown). The very small differences computed for G and C (Supporting Information) are due in part to the small differences in their ribose ring conformation. In this context it is interesting to note that the large differences in CS anisotropy observed for different mononucleotides by solid-state NMR[43] are likely to reflect the substantial differences in ring pucker and glycosidic torsion angles observed in the corresponding X-ray structures.

The 3D NMR pulse sequences described are easily adapted, by removing proton decoupling during one or both indirect evolution periods, for measuring one-bond carbon−proton RDCs for the ribose moiety, even in the generally very crowded C2′, C3′, C4′, and C5′ regions of the spectrum.

Finally, it is interesting to note that, although the experimental NMR measurements presented here are carried out in isotropic and weakly aligning media, this method allows us to extract the complete magnitude and orientation of the CS tensors, in full analogy with NMR measurements performed on single crystals. While a thorough single-crystal study offers very high accuracy and precision, the growth of single-crystals of biological macromolecules of a size suitable for such studies is generally not feasible. Importantly, the liquid crystal method also has the advantage, for biological molecules, of providing tensors which are directly reflective of and applicable to the physiological conditions and conformation experienced by the molecules in solution.

Supporting Information Available: Full ref 53; six tables showing further quantum chemical calculated chemical shift tensors results; one table showing the direction cosines relating experimental and calculated CS tensor orientations; one table showing the effect on the CS tensors of adding random noise to the experimental $\Delta\delta$ data. This material is available free of charge via the Internet at http://pubs.acs.org.

JA051039C

(67) Rossi, P.; Harbison, G. S. *J. Magn. Reson* **2001**, *151*, 1−8.
(68) Ebrahimi, M.; Rossi, P.; Rogers, C.; Harbison, G. S. *J. Magn. Reson* **2001**, *150*, 1−9.
(69) Boisbouvier, J.; Brutscher, B.; Pardi, A.; Marion, D.; Simorre, J. P., *J. Am. Chem. Soc.* **2000**, *122*, 6779−6780.
(70) Dejaegere, A. P.; Case, D. A., *J. Phys. Chem. A* **1998**, *102*, 5280−5289.
(71) Scott, L. G.; Tolbert, T. J.; Williamson, J. R., *Methods Enzymol.* **2000**, *317*, 18−38.

(72) Furtig, B.; Richter, C.; Bermel, W.; Schwalbe, H., *J. Biomol. NMR* **2004**, *28*, 69−79.